Vertical propagation of the extra-tropical Rossby wave during the El Niño 1997/98 off the west coast of South America in a medium-resolution OGCM simulation

Marcel Ramos (1), Boris Dewitte (2) Oscar Pizarro (3) and Gilles Garric (4)
(1) CEAZA-UCN, (2) LEGOS/IRD/CNES-Francia (3) DGO/COPAS-UDEC (4) MERCATOR-OCEAN-Francia

Abstract: The vertically propagating variability along the coast of Peru-Chile is investigated from a medium-resolution OGCM simulation focusing on the strong 1997/98 El Niño event. Diagnostics based on classical linear theory extended here for treating the extra-tropical latitudes reveal the signature of vertically propagating wave at interannual timescale all along the coast. Consistently with theory, the energy 'beams' associated to the interannual extra-tropical Rosbby wave (ERW) slope westward/downward more in the South than in the North. At 15ºS and 30ºS, this process is confined to the ~800 and ~250 km near the coast respectively. The analysis also reveals that the peak phase of the El Niño event along the equator is associated to negative vertical displacements of the isotherms (a rise) along the ray paths, which is due to the peculiar vertical structure variability near the coast and the impact of the higher-order baroclinic mode equatorial Kelvin waves that become more energetic as El Niño develops.

Model configuration and forcing:

We used an ocean general circulation model (OGCM) simulation for 1992-2001 of the MERCATOR global model. The eddy permitting ¼° global MERCATOR model is based on the primitive equations global general ocean circulation model OPA, written by [Madec et al., 1998].

The horizontal resolution based on an ORCA-type grid gets finer with increasing latitudes: ~27.75 km at the equator, ~13.8 km at 60°S or 60°N. This configuration has 46 vertical z-levels. This ¼° configuration is based on the 8.2 version of OPA, with a free surface formulation, isopycnal diffusion for temperature and salinity, biharmonic horizontal viscosity with an added harmonic operator in the equatorial (1-3° latitude) upper layers for the dynamics, non linear bottom boundary friction, free slip lateral boundary condition, a 1.5 turbulent eddy kinetic energy closure scheme and a convection parameterized by enhanced vertical mixing coefficient.

The bathymetry is derived from the Etopo2. A relaxation of 40 w.m^{-2} is applied towards the Real-time, global, sea surface temperature daily analysis and the Levitus *et al.* [1998] monthly climatology of sea surface salinity. The freshwater discharge from continents is represented by 120 river mouths inflows. Daily surface atmospheric conditions are given by the ECMWF reanalysis project. The experiment started at rest from the 1st January 1992 with prescribed conditions for temperature and salinity derived from the Levitus *et al.* [1998] data set for the middle and low latitudes. The year 1992 has been integrated three times before launching the interannual experiment over the 1993-2001 period. The simulation is referred as POG05B hereafter [see Derval et al., 2005, for more details].

Data set and Methods:

In order to validate the propagation properties of the simulation, sea level height (SLH) anomalies were obtained from TOPEX/Poseidon, ERS-1/2 and Jason-1 data sets (TPERSJ) from October 1992 to January 2005. The SLH global maps result from an optimal interpolation of combined altimetry data on a Mercator 1/3° grid every week. SLH anomalies are computed with respect to a seven-year mean (January 1993 to January 1999). In addition, global-scale gridded data of temperature and salinity from the World Ocean Atlas 2001 (WOA01) were used to estimate the theoretical phase speed (standard and extended theory) of subtropical Rossby waves [Killworth et al., 1997].

The methodology adopted in this study follows to a large extent Kessler and McCreary (1993). It uses the Wentzel-Kramers-Brillouin (WKB) ray path theory as a tool to interpret wave features identified in vertical isotherm displacements in the equatorial wave guide. The theoretical background of the WKB ray path theory and the range of validity of the assumptions made are generalized for the extra-tropical latitudes and the 'adapted' formalism is presented in the Appendix. Following Kessler and McCreary (1993), isotherm vertical displacements are derived from the simulated temperature field interpolated vertically on a 5 m grid using 1-D cubic splines. This field is projected on the baroclinic mode structures for vertical velocity and the contribution of the summed-up contribution of first three baroclinic mode is derived.

Here since we focus on the 1997/98 El Niño and cannot extract a single dominant interannual frequency representative of this event over the relatively short record of the simulation, Complex Empirical Orthogonal Functions (CEOF) following the method of Horel [1984] are used to evaluate the spatial patterns and temporal evolution of the dominant modes of variability at interannual timescales during this period.

In order to focus on interannual anomalies, all time series (altimetry data and simulated fields) are previously low-pass filtered with a Cosine-Lanczos filter (50% power at 18.4 months) after extracting the seasonal cycle. The seasonal cycle was derived by least square fit of the time series to the annual and semiannual harmonics.

Extra-tropical Rossby wave characteristics:

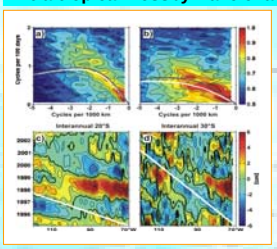

At interannual timescales, theory predicts that ERW can radiate at any latitude along the coast. Indeed, westward propagation of sea level anomalies can be clearly observed in the Eastern South Pacific at interannual timescales. However , a fast decay of the signal near the coastal boundary is observed, mainly for the 1997/98 El Niño (Figure 1).

In our study, we focus on one particular process which is the vertical propagation of energy associated to ERW. Such process is often claimed as the one responsible for the decrease in amplitude of the ERW as they propagate off-shore.

The motivations for focusing on this particularly strong event are also related to the fact that: 1) it may ease the identification of vertically propagating energy that involves the slow high-order baroclinic mode ERWs; 2) it was well documented in the literature for the equatorial region in particular with respect to its vertical structure variability, which provides material for the interpretation the results presented in this study.

Figure 1. 2-D spectrum for sea level anomaly from TPERSJ at 20°S (a) and 30°S (b), respectively (each spectrum has been calculated from the coast to 160° W). The thick lines in the spectrum are the dispersion curves for the standard theory (lower white lines) and the extended theory (upper grey lines) for the first-mode baroclinic RW. Longitude-time diagrams of the interannual sea level anomaly from TPERSJ at 20°S (c) and 30°S (d), respectively. The white lines represent the (standard) theoretical phase for the first vertical mode of a long RW.

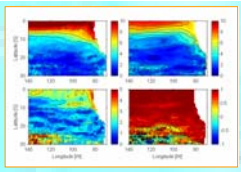

Figure 2. Eastern South Pacific study area. Standard deviations (in cm) of the interannual sea level anomaly from combined TPERSJ product (left upper panel) and MERCATOR model (right upper panel). Standard deviations (in cm) of the differences between the model and the observations (left lower panel). Temporal correlations between the model and the observations (right lower panel).

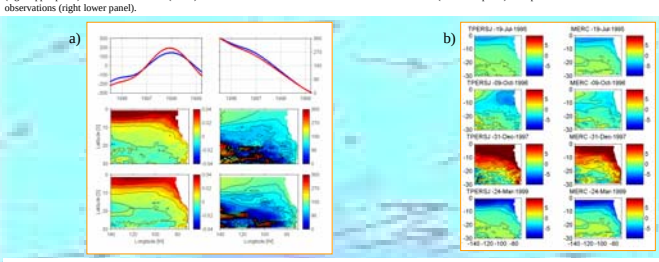

Figure 3. (a) CEOF analysis of the interannual sea level anomaly from TPERSJ and MERCATOR model. Time sequences of first-mode real amplitudes (left upper panel) and phases (right upper panel). The blue line is MERCATOR and red line is TPERSJ. Spatial patterns of first-mode real components (left middle panel) and phases (right middle panel) from TPERSJ. (Lower panels) Same as middle panels but from MERCATOR model. Percentages of variance explained by the first-mode CEOF of TPERSJ and MERCATOR patterns are 95% and 93%, respectively. (b) Reconstructed (left panels) TPERSJ and (right panels) MERCATOR interannual anomalies calculated from first-mode CEOF (Figure 3.a).

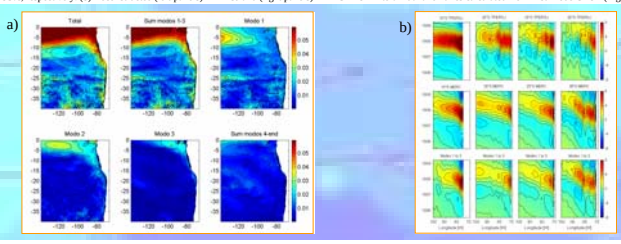

Figure 4. (a) Contribution of sea level for the first three baroclinic modes from MERCATOR model (RMS in cm).. (b) Longitude-time diagrams of the reconstructed (upper panels) TPERSJ and (middle panels) MERCATOR interannual anomalies calculated from first-mode CEOF (see Figure 3). (Lower panels) Same as middle panels but the interannual anomalies are the contribution of the first three baroclinic modes. In this case, the percentage of variance explained by the first-mode CEOF is 94%.

The model sea level variability is compared to the altimetric data. The comparison reveals an overall similar pattern over the study region with maximum variability in the equatorial band and a sharp southward decrease near 10°S more marked in the model than in the observations (Figure 2). The spatial patterns of amplitude and phase for the model and the observations are comparable, furthermore the associated time series for the model and the observations are highly correlated (Figure 3). The maps of phase reveal westward propagations south of ~10°S with the phase speed decreasing southward. It is interesting to note that the results of the vertical mode decomposition accounts for a large variance the variability, which provides a consistency check for the interpretation of the model variability in terms of propagating ERW. The contribution of the first three baroclinic modes to the sea level variability account for 69%, 64%, 78% and 83% of the variance of the total sea level variability at 15°S, 20°S, 25°S and 30°S respectively (Figure 4.b). The comparison between the model results and the observations indicates that the propagation characteristics of the interannual ERW during the 1997/98 El Niño event are comparable.

Vertically propagating energy:

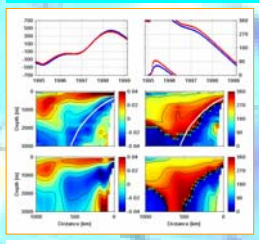

The zonal section for the amplitude for the isotherm displacements suggests two domains separated by a slanted line extending roughly from the coast at 400 m to the west up to 1500 m. Above and to the west of this line, the maximum amplitude is found within the thermocline where WKB theory is not expected to apply. Below, the zone of maximum amplitude is located around the WKB ray path and the phase lines are approximately parallel, with phase propagating upward and westward, and their slope more steeply downward at depth, where the stratification is weaker. Comparable features are observed for the summed-up (baroclinic modes 1 to 3) contribution to isotherm vertical displacements.

Figure 5. CEOF analysis of the interannual isotherm vertical displacements from MERCATOR model at 20ºS. Time sequences of first-mode real amplitudes (left upper panel) and phases (right upper panel). The blue line is total contribution and red line is the contribution of first three baroclinic modes. Spatial patterns of first-mode real components (left middle panel) and phases (right middle panel) from total contribution of MERCATOR. The thick white lines indicate the theoretical ray paths (see text). (Lower panels) Same as middle panels but is the contribution of the first three baroclinic modes. Percentages of variance explained by the first-mode CEOF of total contribution and baroclinic modes patterns are 83% and 84%, respectively.

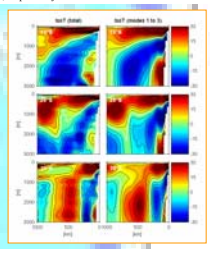

Figure 6. Sections of the isotherm vertical displacements at 15°S, 20°S and 30°S, reconstructed from first-mode CEOF and estimated around of the maximum sea level of El Niño event, i.e. January 1st 1998 (see Figure 3 and text). (Left panels) The total contribution and (right panels) of the first three baroclinic modes from MERCATOR model (see text). Units are m. Percentages of variance explained by the first-mode CEOF are 87% (90%), 83% (84%) and 75% (77%) for the total contribution (the first three baroclinic modes) at 15°S, 20°S and 30°S respectively.

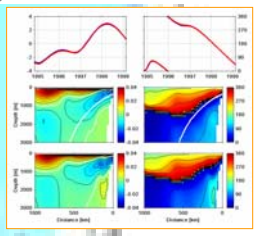

Figure 7. CEOF analysis of the interannual pressure perturbation from MERCATOR model at 20ºS. Time sequences of first-mode real amplitudes (left upper panel) and phases (right upper panel). The blue line is total contribution and red line is the contribution of first three baroclinic modes. Spatial patterns of first-mode real components (left middle panel) and phases (right middle panel) from total contribution of MERCATOR. The thick white lines indicate the theoretical ray paths (see text). (Lower panels) Same as middle panels but is the contribution of the first three baroclinic modes. Percentages of variance explained by the first-mode CEOF of total contribution and baroclinic modes patterns are 91% and 92%, respectively.

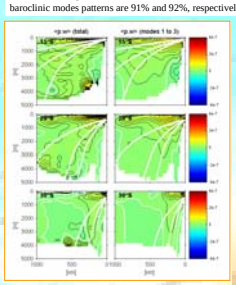

We compute the vertical flux through a unit horizontal area Ev = <*p.w*>, where *w* is obtained from the time derivative of the formerly derived vertical isotherm displacements and *p* is the pressure "deviation", and the brackets refer to an adequate time average, at 15°S, 20°S and 30°S.

We use the CEOF dominant mode instead of a specific harmonic of the pressure and estimated vertical velocity to estimate the <*p.w*>. The time averaging is done over the ENSO cycle as derived from the CEOF analysis of sea level (Figure 3.a). Note that similar results are obtained considering the harmonics at the 3.7 year period, with however less amplitude for the resulting flux.

The results indicate that some energy is transmitted through the thermocline, although this flux is decreasing rapidly with depth with a sharper trend in at 30°S than at 15°S. The pattern of the summed-up contribution of the first three baroclinic modes exhibit similar characteristics than the 'full' vertical energy flux, consistently with the interpretation of the variability in terms of propagating standing modes.

Figure 8. Sections of the vertical energy flux for the interannual signal at 15°S, 20°S and 30°S. (Left panels) The total contribution and (right panels) of the first three baroclinic modes from MERCATOR model (see text). The thick white lines indicate the theoretical ray paths for phase speed values of the first three baroclinic modes. Units are m2s-2. Positive values are for downward flux.

Conclusions:

- Diagnostics based on classical linear theory extended here for treating the extra-tropical latitudes reveal the signature of vertically propagating wave at interannual timescale all along the coast.

- Consistently with theory, the energy 'beams' associated to the interannual ERW slope westward/downward more in the South than in the North.

- The analysis reveals that the peak phase of the El Niño event along the equator is associated to negative vertical displacements of the isotherms (a rise) along the ray paths, which is due to the peculiar vertical structure variability near the coast and the impact of the higher-order baroclinic mode equatorial Kelvin waves that become more energetic as El Niño develops.

- We concluded that great part of the decay observed in the interannual sea level near the coastal boundary is due to the vertical propagation of energy.

Appendix: Linear formalism for vertically propagating extratropical Rossby waves

The linear, inviscid equations for a β-plane ($f=f_0+\beta y$) can be separated into vertical an horizontal components. The horizontal component yields a dispersion relation for standin wave modes in the meridional and horizontal direction $\omega = \frac{-\beta k}{k^2+l^2+f_0^2/c_n^2}$ (A1)

where l and k is the meridional and zonal wavenumbers respectively, ω the frequency; f_0 th Coriolis parameter at some latitude at and c_n the separation constant of the vertical structur equation: $\frac{d}{dz}\left(\frac{d\Psi_n}{dz}N^{-2}\right)+\Psi_n c_n^{-2} = F \quad + \quad$ B.C. (A2)

N is the local Brunt-Vaisala (or buoyancy) frequency and F is the projection of the forcing.

From the vertical equation a local vertical wavenumber can be defined:

$$m_n(x,z) = \frac{N(x,z)}{c_n(x)} \quad \text{(A3)}$$

We now consider a motion which is the combination of the solutions of the different vertical modes for a specified m the local vertical wavenumber. It is then interesting to describe the solution as if the vertical scale m^{-1} of the wave was small compared with the scale on which m varies (WKB approximation). (A1) is then a relation between ω, m and k which can be differentiated to estimate group velocities. In this study, we consider only long zonal wavelengths. In this limit ($k^2+l^2 \approx 0$), the dispersion relation reduces to $\omega = -\frac{\beta k c_n^2}{f_0^2}$ (A4)

Given the wave frequency and phase speed, the trajectory that defines wave energy propagation can be obtained by integrating two ordinary differential equation:

$\frac{dx}{dt} = C_{xg} = \frac{\partial \omega}{\partial k}$ and $\frac{dz}{dt} = C_{zg} = \frac{\partial \omega}{\partial m}$. The slope of ray paths in the (x,z) plane becomes:

$\frac{dz}{dx} = \frac{c_{zg}^2}{c_{xg}^2} = 2\frac{\omega f^2}{\beta c N}$ (A5)

Therefore the wave energy originating at the surface propagates downward toward the west with steeper slope for weaker stratification or lower latitude.

Acknowledgements: M. Ramos was supported by a scholarship and a thesis scholarship (AT-4040200) from Chilean National Research Council (CONICYT). The preparation and development of this work were made possible thanks to several stays funded by ECOS (grants N# C03U05) of B. Dewitte, O. Pizarro and M. Ramos at PROFC and LEGOS. The authors would like to thank Dr. Aldo Montecinos for his contribution in the use of method CEOF.